THE ASTROPHYSICAL JOURNAL, 242:260–282, 1980 November 15

MOMENTUM AND ENERGY DEPOSITION IN LATE-TYPE STELLAR ATMOSPHERES AND WINDS

L. HARTMANN
Harvard-Smithsonian Center for Astrophysics

AND

K. B. MACGREGOR
Harvard-Smithsonian Center for Astrophysics; and Enrico Fermi Institute, University of Chicago
Received 1980 February 19; accepted 1980 May 19

ABSTRACT

We have calculated the response of the outer atmospheres of cool, low-gravity stars to the passage of the mechanical energy fluxes of solar magnitude in the form of acoustic waves and Alfvén waves. The acoustic (or magnetic fast mode) waves dissipate through shock formation in the low chromosphere; while they can account for the temperature and density structure of chromospheres, such waves have damping lengths that are too short to be effective in driving mass loss. Alfvén waves are efficient in generating outflow, and can account for the order of magnitude of observed mass loss in late-type luminous stars. However, unless these magnetic waves undergo some dissipation within several stellar radii of the surface, the predicted terminal velocities of the resulting stellar winds are far too high. Frictional dissipation and the other mechanisms suggest that dissipation may occur, but the magnitude of the effect is not certain. Alfvén wave dissipation should give rise to extended warm chromospheres in low-gravity, late-type stars, a prediction which can be observationally tested.

For fixed magnetic field strength and Alfvén wave energy flux, the mass loss rate increases with decreasing gravity. With assumed masses and radii typical of late type stars, and with energy fluxes of 3×10^6 ergs cm^{-2} s^{-1} and field strengths $\sim$10 gauss, we find mass loss rates that are consistent with observational estimates.

The temperatures of the extended chromospheres should increase with increasing stellar gravity. At high gravities the dissipation of Alfvén waves results in heating the outer atmosphere to coronal temperatures. Thus we cannot obtain self-consistent, low-temperature, low-velocity winds for $\log g \gtrsim 2$. This constraint is consistent with recent work on the transition from solar-type winds to cool winds in the H-R diagram. It is suggested that Alfvén wave dissipation results in coronal heating at high gravities and mass loss at low gravities.

Subject headings: stars: atmospheres — stars: chromospheres — stars: coronae — stars: late-type — stars: mass loss — stars: winds

I. INTRODUCTION

Mass loss from late type stars occurs in at least two distinct modes, depending upon the stellar gravity. The Sun ejects material in a high velocity, tenuous, hot flow. Supergiants, on the other hand, have massive cool winds with terminal velocities $\sim$10–50 km s^{-1}, well below the surface escape velocity (Deutsch 1956, 1960; Weymann 1962). The behavior of the winds of stars of intermediate gravity is not well understood at this time (cf. discussions by Reimers 1977*a* and Stencel 1978). Hartmann, Dupree, and Raymond (1980) have recently suggested that "hybrid" winds may occur, characterized by the presence of both hot gas and cold circumstellar material, and wind terminal velocities which are intermediate between solar wind velocities and cool supergiant ejection speeds. Recent ultraviolet observations suggest that late-type stars with $\log g \lesssim 2$ do not have transition region ($T \geq 10^5$ K) gas (Wing 1978; Linsky and Haisch 1979). This division of temperature structures in the H-R diagram has been identified with the so-called "supersonic transition locus" of Mullan (1978), where wind properties are thought to undergo a fundamental change, and may mark the division between "hot" and "cool" winds.

The solar wind is basically thermally driven (Parker 1958), although significant modifications of solar wind structure can arise from nonradial magnetic field geometry (Kopp and Holzer 1976) and from the pressure due to propagating Alfvén waves (see, e.g., Belcher 1971; Hollweg 1973; Jacques 1978). The apparent absence of high-temperature gas suggests that this cannot be true of supergiant winds. The most popular explanation of such

winds has been radiation pressure acting on dust grains formed in the outer atmospheric layers (Weymann 1960; Gehrz and Woolf 1971; Kwok 1975). However, this theory has difficulties. It is not clear whether mass loss and dust infrared radiation are empirically correlated (Hagen 1978). In theoretical calculations, it is typically necessary to begin the flow at some large distance above the stellar photosphere in order for the gas to cool sufficiently for dust to form (Kwok 1975), which raises the question of why the atmosphere expands significantly to reach the grain-forming point. Observationally, it has been shown that less than 20% of the dust radiation from α Ori comes from $r < 12\ R_*$ (Sutton *et al.* 1977), and that the outflow appears to be already underway in the chromosphere (Wilson 1960; Dupree 1976), well before grains are likely to form. The most severe disadvantage of the dust-driven wind theory is that it cannot universally account for the observed mass loss in luminous late-type stars. Many stars are of such high effective temperature, or low luminosity (cf. Reimers 1977*a*), that it is extremely doubtful that dust can be dynamically important.

Haisch, Linsky, and Basri (1980) have recently investigated a suggestion due originally to Wilson (1959), that $L\alpha$ radiation pressure can drive mass loss, specifically for the K2 IIIp star α Boo. They calculate a $L\alpha$ flux based on a radiative transfer solution, which neglects velocity gradients. Their results show that $L\alpha$ pressure may be larger than gravity over a small region where $L\alpha$ is optically thin, but that the total momentum added is insufficient to generate mass loss, so that Alfvén waves are ultimately responsible for driving the outflow. Neither mass loss rates nor wind terminal velocities were calculated in this work. The $L\alpha$ mechanism is very sensitive to the ionization state of the gas. If the material is too cold, the $L\alpha$ is so optically thick that the force is negligible; if the gas is too hot, insufficient neutral hydrogen is available to absorb radiation. Since the temperature distribution adopted by Haisch *et al.* is not uniquely determined by the observations (cf. Linsky and Haisch 1979), it is unclear whether the atmospheres of cool luminous stars actually become supersonic from $L\alpha$ radiation pressure.

In this paper we wish to investigate the possibility that universal mechanisms of mechanical energy generation and deposition occur in all late-type stars, and that their specific effects on chromospheric temperature structure and mass loss are modified principally by surface gravity. The discovery of hybrid atmosphere stars (Hartmann, Dupree, and Raymond 1980), possessing a combination of solar and cool supergiant-type characteristics, encourages our application of solar mechanical energy fluxes to low-gravity situations. In particular, the discussion focuses on the behavior of acoustic and magnetic wave modes known to exist on the Sun. These modes can be much more efficient than radiation pressure in driving mass loss. Specifically, for a given energy flux, the wave momentum flux varies inversely as the mode speed, which is typically a factor $\sim 10^4$ smaller than the speed of light. In a sense this is a more direct accounting of the action of the wave modes, for the $L\alpha$ emission presumably results from mechanical energy deposition by waves.

Observations of chromospheric emisson losses in late-type stars suggest that the acoustic wave energy fluxes per unit area are roughly independent of gravity (Linsky and Ayres 1978). From this starting point we construct model chromospheres considering the energy and momentum deposition due to shock waves. Our results show that the behavior of shock energy deposition as a function of gravity may be important in determining the presence or absence of transition regions, and in setting the base temperature of cool winds. However, the distance scales over which shocks are dissipated are too short to be effective in driving mass loss for any but the lowest-gravity stars. The similarity of the magnitude of acoustic wave energy fluxes in the Sun and other stars suggests that Alfvén wave energy fluxes of solar magnitude (Jacques 1978) may also be present in supergiants. Our calculations show that large mass loss rates may be accounted for by the effects of Alfvén waves. A discussion of the physical circumstances under which these magnetic waves result in low velocity winds forms the final section of the paper.

II. ACOUSTIC WAVE ENERGY DEPOSITION IN STATIC ATMOSPHERES

It is generally believed that dissipation of acoustic waves heats the lower chromospheres of late-type stars (cf. Ulmschneider 1970; Renzini *et al.* 1977; De Loore 1968). Ulmschneider *et al.* (1977) and Ulmschneider, Schmitz, and Hammer (1979) have carried out detailed, time-dependent hydrodynamic calculations of chromospheric heating. From the wide variation of chromospheric activity at a given position in the H-R diagram, and from the correlation of solar surface activity with magnetic fields, it appears that magnetic activity is closely connected with chromospheric mechanical energy generation (cf. Skumanich 1972), and that magnetic waves should be present along with acoustic waves. However, Osterbrock (1961) has shown that for moderate field strengths in the low chromosphere, fast-mode magnetic shocks will dissipate essentially as acoustic shocks. Thus we ignore the possible magnetic character of these waves in order to avoid having to specify the magnetic field strength.

In this section we consider an approximate, time-averaged treatment of acoustic shock wave damping which enables us to extend the heating calculations to supergiant gravities. This discussion is based on a newly available, accurate, solar radiative cooling law obtained from Dr. E. Avrett (private communication). From these calculations we can examine the behavior of shocks in low-gravity circumstances.

a) Radiative Cooling Rates

In order to determine the temperature distribution, we must estimate the radiative cooling rate. The exact solution for the cooling is in general an iterative process, for optical depth effects play a role in the escape of radiation from such important lines as the Mg II and Ca II resonance transitions (cf. Giovanelli 1978). This would prevent us from simply integrating the hydrostatic equilibrium and energy equations outward from the temperature minimum. We adopt instead a cooling rate which is a function of density and temperature alone, based on a derived solar cooling rate; however, we adjust the cooling rates to take into account the larger Mg II and Ca II optical depths, and hence lower escape probabilities, encountered in low-gravity stars.

The H^- cooling can be computed in the optically thin limit. Following Kalkofen and Ulmschneider (1979), we use the approximation that bound-free processes dominate the H^- heating and losses. Then the radiative losses are

$$\Lambda_{H^-} = 4\pi N^*_{H^-} \int_{\nu_0}^{\infty} d\nu\, \alpha_{bf}(\nu) W(\nu, T) \left[1 + \frac{c^2}{2h\nu^3} J(\nu) \right] \equiv N^*_{H^-} E, \tag{1}$$

where α_{bf} is the bound-free cross-section, $W(\nu, T)$ is the Wien function, $J(\nu)$ is the mean intensity of the photospheric radiation field, and $N^*_{H^-}$ is the LTE H^- number density, given by

$$N^*_{H^-} = 2.89 \times 10^{-22} N_e N_{H\,I} \theta^{1.5} e^{1.736\theta}, \tag{2}$$

with $\theta = 5040/T$. Equation (1) results from the detailed balance relation between radiative recombination and photoionization.

The heating due to absorption of photospheric radiation is

$$\Gamma_{H^-} = 4\pi N_{H^-} \int_{\nu_0}^{\infty} d\nu\, \alpha_{bf}(\nu) J(\nu) \equiv b N^*_{H^-} H, \tag{3}$$

where b is the H^- departure coefficient. In order to calculate b, we require the photoionization rate R_i, and the recombination rate R,

$$R_i = 4\pi \int_{\nu_0}^{\infty} d\nu \alpha_{bf}(\nu) \frac{J(\nu)}{h\nu}, \tag{4}$$

$$R = 4\pi \int_{\nu_0}^{\infty} d\nu \alpha_{bf}(\nu) \frac{W(\nu, T)}{h\nu} \left[1 + \frac{c^2 J(\nu)}{2h\nu^3} \right]. \tag{5}$$

Then

$$b = \frac{R + \Gamma N_{H\,I}}{R_i + \Gamma N_{H\,I}}, \tag{6}$$

where $N_{H\,I}$ is the neutral hydrogen density and $\Gamma = 2.1 \times 10^{-9}$ cm^3 s^{-1} is the associative detachment coefficient (Vernazza, Avrett, and Loeser 1973).

Because H^- is optically thin, for a plane-parallel geometry we may compute all of these quantities once for a given photospheric radiation field. For concreteness we have chosen $T_{eff} = 4250$ K, so that $J(\nu) = \frac{1}{2} B(\nu, T_{eff})$, with $B(\nu, T)$ the Planck function. Numerical integrations, using the cross section given by Gingerich (1964) as corrected by Ulmschneider and Kalkofen (1978), can then be matched by the following fits, which are accurate to within a few percent;

$$3000 \leq T \leq 4500 \text{ K}; \; E = 3.266 \times 10^{-7} (T/3000)^{4.8269} \text{ ergs s}^{-1}, \tag{7}$$

$$R = 1.581 \times 10^5 (T/3000)^{4.4214} \text{ s}^{-1}; \tag{8}$$

$$4500 \leq T \leq 7000 \text{ K}; \; E = 2.312 \times 10^{-6} (T/4500)^{3.9769} \text{ ergs s}^{-1}, \tag{9}$$

$$R = 9.495 \times 10^5 (T/4500)^{3.4941} \text{ s}^{-1}; \tag{10}$$

and

$$H = 9.088 \times 10^{-7} \text{ ergs s}^{-1}; \; R_i = 3.840 \times 10^5 \text{ s}^{-1}. \tag{11}$$

The net radiative cooling due to H^- is $\Lambda_{H^-} - \Gamma_{H^-}$, which is a function of T, $N_{H\,I}$, and the electron density N_e.

Avrett (1979, private communication) has recently used the PANDORA computer code (Vernazza, Avrett, and Loeser 1973 [VAL]) to calculate the radiative losses in the standard VAL solar model. The dominant losses for $T \leq 10^4$ K are mainly due to Mg II h and k, Ca II H and K, and Ca II infrared triplet lines; for $T \geq 10^4$ K, hydrogen continua and lines are most important. The resulting cooling function is summarized in Table 1. These calculations show that H^- is much less important in cooling than usually thought near the temperature minimum; presumably line blanketing processes, such as CO, become important. For simplicity we use the H^- cooling as representative of the low-temperature losses, since the treatment of line blanketing is complex and uncertain. In addition, the H^- losses in our models are much greater at, say, 5000 K than in the Sun, because of the much lower effective temperature adopted.

While these cooling rates depend on optical depths, and hence on the assumed structure, as an initial approximation we take this cooling rate to be formally a function only of density and temperature for the purposes of calculation. Then, for solar-gravity stars, the energy equation is

$$\frac{dF_m}{dZ} = -(\Lambda_R + \Lambda_{H^-}) + \Gamma_{H^-}, \tag{12}$$

where $\Lambda_R = N_e N_H P_{R\odot}(T)$ is determined from Table 1, and dF_m/dz is the mechanical heating rate per unit volume (cf. § IIc).

For low surface gravity giants and supergiants, we expect larger scale heights, and consequently larger chromospheric mass column densities (i.e., thicker chromospheres). Observationally, this is indicated by the Wilson-Bappu relation (Ayres, Linsky, and Shine 1975; Ayres 1979). Thus, collisionally excited lines which provide the dominant cooling at $T \leq 8000$ K should have increased optical depths, and the cooling rate due to such lines will be reduced. Note that this should not affect H^-, which remains optically thin in any case, nor should it affect the cooling rate at $T > 8000$ K (due to Lyman lines and continuum) since at these temperatures the Lyman continuum is optically thin. Ayres, Linsky, and Shine (1975) (see also Ayres 1979) deduced that the chromospheric mass column density at T_{min} empirically scales as $m \sim g^{-1/2}$ in order to account for the Wilson-Bappu effect. We therefore assume that the optical depths of lines formed in the region $5000 \leq T \leq 8000$ K scale as $\tau \sim m \sim g^{-1/2}$. In this region, photons emitted in the optically thick line cores diffuse in frequency, ultimately escaping in the damping wings of the line, where the escape probability P_{esc} scales as $P_{esc} \sim \tau^{-1/2} \sim g^{1/4}$. This accounts only for direct escape of radiation. Thermalization effects may be important but are probably not greater than the uncertainties in our derived electron densities. To account for reduced line cooling in low-gravity stars at $T \leq 8000$ K, we correct the previously deduced solar radiative cooling coefficient $P_{R\odot}(T)$ by a multiplicative factor of P_{esc}, according to

$$P_R(T) = P_{R\odot}(T)(g/g_\odot)^{0.25}, \tag{13}$$

for $T \leq 7160$ K. For $T > 8000$ K, the Mg II and Ca II lines in the Sun become optically thin, so that the escape probability increases rapidly outward. Furthermore, cooling in hydrogen becomes increasingly important with higher temperatures. Detailed calculations show that the Lyman continuum becomes optically thin near 8000 K for model

TABLE 1

SOLAR RADIATIVE COOLING RATE

T(K)	P_R(ergs cm^3 s^{-1})
5030.....	5.77E−27
5650.....	1.62E−26
6040.....	4.57E−26
6440.....	1.35E−25
7160.....	3.22E−25
8440.....	1.01E−24
9500.....	2.16E−24
10700....	2.86E−24
12300....	6.60E−24
18500....	5.03E−23
22500....	5.90E−23

chromospheres with a wide range of $\log g$, mainly because hydrogen generally becomes substantially ionized in this temperature region (cf. Baliunas *et al.* 1979). We therefore expect the cooling rate to be relatively independent of optical depth for $T > 8000$ K, and to approach the solar value with increasing temperature. The adopted cooling law for all gravities sets $P_R = P_{R\odot}(T)$ for $T \geq 8440$ K. At intermediate temperatures, $P_R(T)$ was determined from a power law fit through the values at $T = 7160$ K and $T = 8440$ K.

b) Ionization Equilibrium

Calculation of the cooling rates requires a knowledge of the electron density as a function of total density and temperature. For the purposes of these chromospheric calculations we develop a simple approximation consistent with the spirit of the approximate cooling law derived in the previous section.

The electron population is assumed to arise from two components, the first being single ionization of metals. This is approximated by a constant contribution to the electron number density $A_m N_{\rm H} \approx 1 \times 10^{-4} N_{\rm H}$, where A_m is the metal abundance by number relative to hydrogen; this assumes solar abundances. The second component is due to the ionization of hydrogen. The proper calculation of this is complex, but simple approximations can be made which result in a reasonable balance.

For temperatures well below 8000 K, the Lyman continuum and lines are very optically thick, and approach radiative detailed balance. Collisional processes then connect the $n = 1$ and $n = 2$ levels, so that these level populations are related by the Boltzmann factor. (Model chromosphere calculations for the Sun and Arcturus bear out this argument [Avrett, private communication], showing that $b_1 \approx b_2$ in this temperature range.) In this case ionization occurs by photoionization out of the $n = 2$ level due to the stellar photospheric radiation. On the other hand, for $T > 8000$ K the Lyman continuum is optically thin (cf. Baliunas *et al.* 1979), so Lyman continuum photoionizing radiation from underlying, denser layers will dominate the ionization.

Assuming as before that the stellar photospheric radiation field can be represented by a Planck function of radiation temperature T_R, the photoionization rate from the nth hydrogen level (for a ν^{-3} continuum opacity approximation) is

$$\beta_n = \frac{8\pi W}{h^3 c^2} \sigma_{n0} I_n^3 E_1(I_n/kT_R), \tag{14}$$

where I_n is the ionization potential from level n, σ_{n0} is the threshold cross section, $W = \frac{1}{2}$ is the dilution factor, and E_1 is the first exponential integral. From radiative detailed balance, the recombination rate is

$$\alpha_n = \frac{8\pi\sigma_{n0}}{c^2} \frac{n^2 I_n{}^3}{(2\pi m_e kT)^{3/2}} e^{I_n/kT} E_1(I_n/kT). \tag{15}$$

Ionization equilibrium, assuming only continuum processes operate, requires

$$\frac{N_{\rm H\,II} N_e}{N_n} = \frac{W}{n^2}\left(\frac{2\pi m_e kT}{h^2}\right)^{3/2} e^{-I_n/kT} \frac{E_1(I_n/kT_R)}{E_1(I_n/kT)}, \tag{16}$$

where $N_{\rm H\,II}$ is the number density of protons and N_n is the number density of neutral hydrogen atoms in the nth level. Asymptotically,

$$\frac{N_{\rm H\,II} N_e}{N_n} \approx \frac{W}{n^2}\left(\frac{2\pi m_e kT}{h^2}\right)^{3/2} \frac{T_R}{T} e^{-I_n/kT_R}. \tag{17}$$

We may express this result more conveniently in terms of the departure coefficient $b_n \equiv N_n/N_n^*$,

$$b_n = \frac{T}{WT_R} \exp\left[\frac{I_n}{kT_R} - \frac{I_n}{kT}\right]. \tag{18}$$

In the lower chromosphere, when the Lyman continuum and Lyman and Balmer lines are in radiative detailed balance, $I_n = I_2 = (I_1)/4$, and with $T_{\rm B}$ = Balmer continuum photospheric radiation temperature,

$$b_2 = \frac{T}{WT_{\rm B}} \exp\left[\frac{I_1}{4k}\left(\frac{1}{T_{\rm B}} - \frac{1}{T}\right)\right] = b_1. \tag{19}$$

For high temperatures, where the Lyman continuum becomes optically thin,

$$b_1 \approx \frac{T}{WT_L} \exp\left[\frac{I_1}{k}\left(\frac{1}{T_L} - \frac{1}{T}\right)\right], \tag{20}$$

where T_L is the Lyman continuum radiation field temperature. We expect the Lyman continuum to become optically thin near $\sim$8000 K, as discussed earlier, with a radiation temperature therefore $\sim$7000 K. This suggests a transition between (19) and (20) in this temperature range. We adopt, for an effective temperature of 4250 K, a Balmer continuum brightness temperature of 3800 K (Baliunas and Avrett 1979, private communication); then

$$b_1 = \frac{T}{WT_R} \exp\left[\frac{I_1}{k}\left(\frac{1}{4T_R} + \frac{3}{4T_1} - \frac{1}{T}\right)\right], \tag{21}$$

where

$$\begin{aligned} &T < 6000,\ T_R = 3800,\ T_1 = T, \\ &6000 \leq T \leq 8000,\ T_R = 3800 + 1.60(T - 6000), \\ &T_1 = 6000 + 0.5(T - 6000), \\ &T > 8000,\ T_R = T_1 = 7000. \end{aligned} \tag{22}$$

This formula has (19) and (20) as asymptotic limits.

We have compared the predictions of this formula with detailed radiative transfer calculations for ϵ Eri (K2 V) and α Boo (K2 III) (Baliunas and Avrett 1979, private communication). The agreement is better than a factor of 2 for $T < 7000$ K. At higher temperatures b_1 is substantially underestimated, because we have neglected other processes —e.g., nondetailed balance in Lyman lines. However, hydrogen rapidly becomes totally ionized in this temperature range, so the error is much smaller in the derived electron density, which is the only important quantity as far as the cooling law is concerned. We conclude that the above approximation, including metal ionization, yields a reasonable ionization balance.

c) *Mechanical Energy Dissipation and Method of Solution*

To completely specify the chromospheric energy balance, an expression for the rate of heating resulting from the dissipation of mechanical energy is required. We adopt the formalism of Kuperus (1965; see also de Loore 1968) for weak shock waves, in which the wave energy flux may be written

$$F_m = \frac{4}{3}\rho a^3 \frac{(M^2-1)^2}{(\gamma+1)^2 M}, \tag{23}$$

where M is the Mach number of the shock, ρ is the density, and γ is the ratio of specific heats. For a gas with mean mass per particle μ, $a = (\gamma kT/\mu)^{1/2}$ is the sound speed. The dissipation rate is then

$$\frac{dF_m}{dz} = -\frac{16}{3} \frac{\rho a^2}{P_w(\gamma+1)^2} \frac{(M^2-1)^3}{M^4}, \tag{24}$$

where P_w is the wave period. We neglect radiation damping (Ulmschneider, Schmitz, and Hammer 1979) because we consider only the low-density regions at and above the temperature minimum.

The pressure distribution in the atmosphere is determined from the hydrostatic equilibrium equation,

$$\frac{dP}{dz} = -\rho g + \frac{1}{a}\frac{dF_m}{dz}, \tag{25}$$

where the second term on the right-hand side of (25) represents wave momentum deposition, neglecting the effects of reflection and refraction (Rosner and Vaiana 1977).

With initial values for the total number density, wave period, and incident wave energy flux, equations (24)) and (25) can be integrated outward from the location of the temperature minimum in the following manner. At the base

of the atmosphere, the ionization state of the gas is calculated from the assumed density and a guess for the initial temperature. These results permit us to determine the net radiative cooling rate, and (using the initial value of F_m) to determine the shock Mach number. The mechanical heating rate can then be calculated from equation (24); in general, the value so obtained for dF_m/dz will not satisfy equation (12). Accordingly, a new guess for the temperature is made, and the above steps are repeated until thermal balance is achieved. Equations (24) and (25) can then be integrated once to determine values for the gas pressure and wave flux at the next height. At locations different from that of the temperature minimum, the same procedure as outlined above is followed, with the exception that the local number density is calculated from the pressure and a guess for the temperature.

d) Chromospheric Models

We now require values for the initial wave energy flux and period. Linsky and Ayres (1978) showed that, in a sample of late-type stars, the Mg II surface flux behaved roughly as $F(\text{Mg II}) \approx 6 \times 10^{-5} \times \sigma T_{\text{eff}}^4 \times (T_{\text{eff}}/5000)^{2.8 \pm 2}$. We will consider $T_{\text{eff}} = 4250$ K, to correspond to our H^- cooling law fits, so that $F(\text{Mg II}) \approx 1 \times 10^6 (0.85)^{2.8 \pm 2}$. This presumably is a lower limit to the total mechanical energy flux incident on the temperature minimum. Because of the extremely uncertain exponent, and the fact that losses in other lines and continua are unknown, we simply adopt $F_{m0} = 1 \times 10^6$ ergs cm^{-2} s^{-1} for most models here. The data of Linsky and Ayres (1978) show considerable scatter from the mean relation, but show no evidence for a systematic variation of F_{m0} with g.

Renzini *et al.* (1977) assume that wave periods are restricted by the acoustic cutoff frequency $\omega > a(2h)^{-1}$, where h is the local scale height. In general, they expect the period at which most flux is emitted to be $\sim 10^{-1}$ the acoustic cutoff period. This results in a wave period which scales inversely with gravity, a scaling which we adopt for our basic chromospheric models.

In Figure 1 we display the results of our calculations for three standard models (see also Table 2). The models all have the same acoustic wave energy flux of 1×10^6 ergs cm^{-2} s^{-1}, and each is characterized by a temperature minimum density consistent with the Ayres, Linsky, and Shine (1975) scaling. A wave period of 20 s was adopted for solar gravities (Ulmschneider and Kalkofen 1978), and scaled according to $P_W \propto g^{-1}$ for other gravities. More detailed studies of the solar radiative loss function indicate that although H^- is not as dominant a coolant as supposed by Ulmschneider and Kalkofen, 20 s wave periods are still indicated (Avrett, private communication). The resulting temperature distributions have been plotted as a function of z, the distance above the temperature minimum in units of the base scale height $h = \gamma kT/\mu g$, with $\gamma = 5/3$. It can be seen that the overall effect of lowering the gravity is to lower the temperature at a given z. This behavior is a result of the increasing importance of the force

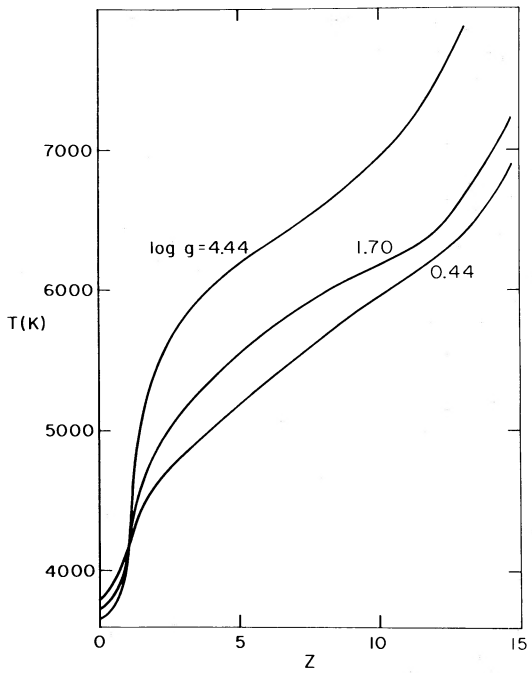

FIG. 1.—Temperature structures of the standard chromospheric models, A, B, and C, plotted as a function of the vertical height in units of isothermal scale heights. Details of the models are listed in Table 2.

TABLE 2

STANDARD CHROMOSPHERIC MODELS ($F_0 = 1 \times 10^6$ ergs cm^{-2} s^{-1})

	MODEL A[a]			MODEL B[b]			MODEL C[c]		
Z	T	N_T	N_e	T	N_T	N_e	T	N_T	N_e
0.0...	3660	2.00(15)	1.82(11)	3729	2.00(14)	1.82(10)	3803	6.00(13)	5.46(9)
0.5...	3715	8.60(14)	7.82(10)	3802	7.95(13)	7.23(9)	3922	2.64(13)	2.41(9)
1.0...	4107	3.53(14)	3.21(10)	4088	3.68(13)	3.37(9)	4154	1.18(13)	1.11(9)
1.5...	5000	1.49(14)	1.76(10)	4594	1.63(13)	1.95(9)	4429	5.51(12)	6.47(8)
2.0...	5367	7.74(13)	1.78(10)	4842	8.15(12)	1.75(9)	4600	2.75(12)	5.44(8)
3.0...	5776	2.44(13)	1.85(10)	5130	2.31(12)	1.53(9)	4821	7.46(11)	4.16(8)
4.0...	6023	8.42(12)	1.66(10)	5346	7.08(11)	1.30(9)	4999	2.17(11)	3.30(8)
6.0...	6316	1.17(12)	1.43(10)	5704	7.80(10)	8.52(8)	5331	2.09(10)	2.10(8)
8.0...	6613	1.89(11)	1.14(10)	5968	1.02(10)	4.73(8)	5666	2.42(9)	1.33(8)
10.0...	6960	3.95(10)	8.65(9)	6168	1.68(9)	2.88(8)	5953	3.73(8)	7.17(7)
12.0...	7472	1.22(10)	5.24(9)	6402	4.06(8)	1.53(8)	6228	9.01(7)	3.69(7)
14.0...	8304	4.87(9)	2.30(9)	6998	1.35(8)	6.38(7)	6674	2.96(7)	1.40(7)
16.0...	9280	2.13(9)	1.01(9)	7426	5.27(7)	2.51(7)	7255	1.08(7)	5.16(6)

NOTE—Numbers in parentheses indicate the power of 10 by which to multiply the preceding number. Z is the distance above the temperature minimum region in units of the base isothermal scale height h.

[a]Model A: $M/M_\odot = 0.64$; $R/R_\odot = 0.80$; $\log g = 4.44$; $P_w = 20$ s; $h = 1.44 \times 10^2$ km.

[b]Model B: $M/M_\odot = 1.33$; $R/R_\odot = 27$; $\log g = 1.70$; $P_w = 10^4$ s; $h = 8.05 \times 10^4$ km.

[c]Model C: $M/M_\odot = 16$; $R/R_\odot = 400$; $\log g = 0.44$; $P_w = 2 \times 10^5$ s; $h = 1.52 \times 10^6$ km.

due to wave dissipation at low gravities. Heating dominates momentum deposition at high gravity, while the waves tend to extend the density distribution and enhance radiative cooling of the gas at low gravity.

The effects of changing wave fluxes and periods are considered for the dwarf gravity case in Figure 2. Increasing the incident wave energy flux changes the temperature structure by a relatively small amount. However, increased dissipation at low heights (and therefore high densities) results in reduced wave fluxes and consequently lower temperatures at large heights. Changing the wave period makes a much greater difference in the temperature

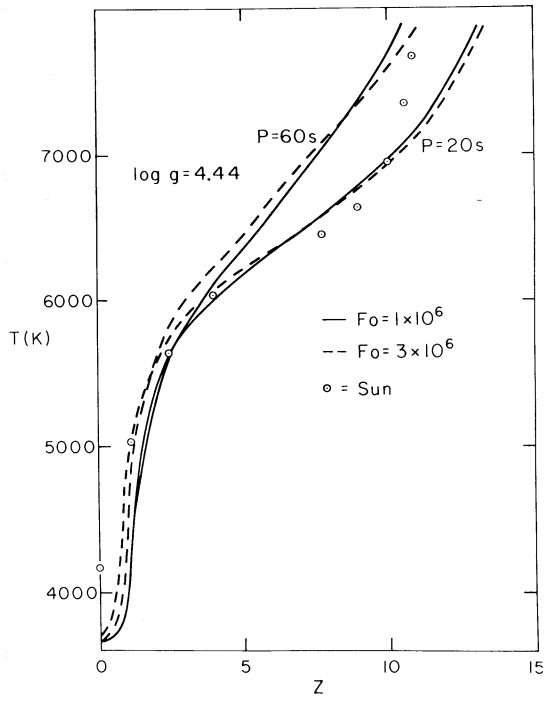

FIG. 2.—Atmospheric responses to differing input shock wave fluxes and wave periods for dwarf gravities. For comparison the solar empirical temperature structure determined by Vernazza, Avrett, and Loeser (1973) has been included.

distribution. For longer-period waves, the dissipation length $L \equiv F_m/(dF_m/dz)$, is larger (cf. eqs. [23] and [24]). As a result, more flux is available for heating at large z, and the temperature is increased.

Also plotted in Figure 2 is the Vernazza, Avrett, and Loeser (1973) solar chromosphere model. The agreement between the empirical model and our 20 s wave model is excellent, except for the extremes of the temperature range. Because the effective temperature is different, and because we have neglected important line blanketing processes near the temperature minimum, we cannot expect the low-temperature calculation to be consistent with observations. Above 7000 K, where the gas becomes substantially ionized, other heating processes may become important. Moreover, we make no provision for treating either wave reflection or heat conduction, which undoubtedly play important roles in determining the occurrence of a transition region. While we cannot therefore determine the position of the transition region, it is clear that a rapid increase in temperature will occur when the calculation is carried to great enough heights. These models, which are similar to the solar results of other authors considering only H^- cooling (Ulmschneider *et al.* 1977; Ulmschneider, Schmitz, and Hammer 1979, and references therein), give us confidence that the approximations made in our treatment are sufficiently accurate to warrant their extension to low-gravity atmospheres.

In Figure 3 we display similar calculations for the giant case. The 1×10^4 s period calculation is comparable to the empirical model temperature structure constructed for α Boo by Ayres (1975). Note, however, that, unlike the results for dwarf gravities, these models exhibit lower temperatures at large z for increasing wave periods. This is caused by the force due to wave momentum deposition which becomes comparable to the gravitational acceleration. This extends the density distribution, permitting the gas to cool more efficiently and attain thermal equilibrium at lower temperatures. Model chromospheres for supergiant gravities show similar properties, as can be seen from Figure 4.

An approximate test for the overall consistency of these chromospheric models can be performed through an analysis of observed chromospheric line widths. Ayres, Linsky, and Shine (1975) and Ayres (1979) have suggested that the modified Wilson-Bappu relation for the Ca II line width $\Delta\lambda(K_1)$ results from a dependence of the chromospheric mass column density on gravity in the form $m \propto g^{-1/2}$. Since $P = mg$ in hydrostatic equilibrium, this relation is equivalent to $P \propto g^{1/2}$, which predicts that in going from $\log g = 4.44$ to $\log g = 0.44$, the pressure at the temperature minimum should decrease by a factor of 100. The actual result of the calculations is a factor ~ 30. In terms of the observed line width, using $\Delta\lambda \propto m^{1/2}$ (Ayres 1979), we find $\Delta\lambda \propto g^{-0.31}$ whereas Ayres (1979) found $\Delta\lambda \propto g^{-0.23 \pm 0.04}$. (Note that the calculated variation of the column density with gravity is not exactly consistent with the cooling law [eq. (13)]; however, the effect on the temperature distribution will be small.)

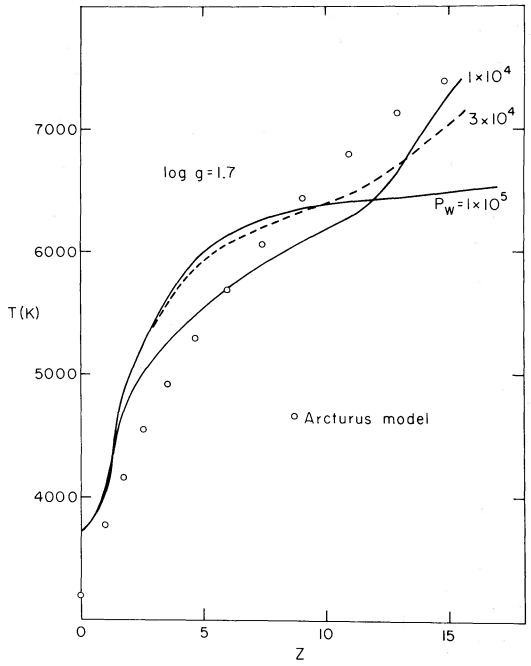

FIG. 3.—Responses of a giant chromosphere to shock waves of differing periods. An empirical chromospheric model which matches the Ca II fluxes has been taken from Ayres (1975). Long-period waves generate momentum deposition comparable to gravity at large heights, which flattens the density distribution and therefore flattens the temperature distribution as well.

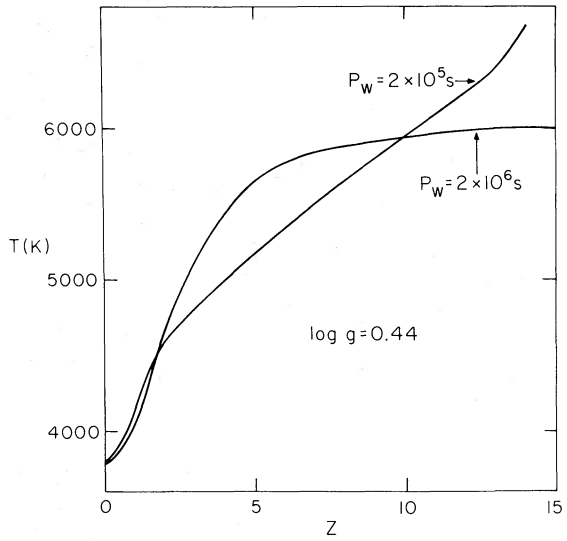

FIG. 4.—Responses of a supergiant chromosphere to different shock wave periods.

We emphasize that Basri (1979) has found that the increasing column density is not capable of reproducing the Wilson-Bappu line widths by itself, but must be accompanied by a turbulent velocity field which is barely supersonic. Such a velocity field may be the result of the shock waves envisaged here, although no quantitative calculations have been made. Despite these complications, it appears that the mass column density must increase with decreasing gravity, and that the Ayres (1979) scaling laws should be a rough guide to the actual behavior of stellar chromospheric column densities.

The approximate consistency of the chromospheric column densities in our models with the observational results can be shown to be primarily due to the scaling of the wave periods with gravity. Consider stars with approximately the same temperature at the temperature minimum. The temperature will begin to rise at a point where the mechanical energy dissipation rate becomes comparable to the background radiative equilibrium terms in the energy equation. If the temperature minimum occurs when dF_m/dz is a fraction f of the background radiative losses, then

$$fN_{\rm H}N_e P_R(T_{\rm min}) \propto fP^2 P_R(T_{\rm min}) \propto \frac{dF_m}{dz}, \tag{26}$$

where we have assumed $N_e = 10^{-4} N_{\rm H}$, and a constant, given temperature ($T_{\rm min}$).

At $T_{\rm min}$ we may approximate dF_m/dz by F_{m0}/L, where L is the local damping length. L is a function of Mach number and is linearly proportional to the wave period P_w (see eq. [24]). If f is a given constant, then from (26) we have

$$P^2 = m^2 g^2 \propto F_{m0}/P_w. \tag{27}$$

Since we have assumed $P_w \propto g^{-1}$ and F_{m0} = constant, we arrive at the desired result $m \propto g^{-1/2}$. The calculations depart from this relation somewhat because the initial Mach number varies for different stellar gravities. This analysis is similar to that of Ayres (1979), but differs in emphasizing the importance of the variation of the dissipation length L.

The results of these chromospheric calculations suggest that the g^{-1} scaling for P_w is approximately correct, both in terms of the comparison of the giant model with the semiempirical Arcturus model and in the rough agreement with the Wilson-Bappu effect. This conclusion is relatively independent of the form of the adopted cooling law, for waves with $L \ll h$ will dissipate too rapidly to form an outward temperature rise, while waves with $L \gg h$ extend the density distribution and reduce the temperature gradient. This scaling law for acoustic shock wave periods has important implications for the ability of shock waves to drive mass loss, as discussed in the following section.

The treatment of this section has neglected the effect of mass loss, which will extend the density distribution and modify the temperature profile at large distances. For example, a typical estimated supergiant mass loss rate is $\approx 10^{-6} M_\odot$ yr^{-1}; assuming a sonic point near the surface, the sonic density would be $\sim 4 \times 10^9$ cm^{-3} for the adopted supergiant parameters. This density occurs in the standard supergiant model at 7.2 scale heights above the

temperature minimum, with $T=5580$ K. It is therefore clear that any discussion of temperatures ≥ 6000 K in supergiant chromospheres is inadequate without consideration of the effects of mass loss. A similar conclusion may apply to the giant chromospheres, based on the mass loss estimates of Chiu *et al.* (1977).

Observations show that there is a considerable range of chromospheric activity for stars at a given position in the H-R diagram (cf. Linsky and Ayres 1978). The level of activity is related to rotation, which presumably affects the chromospheric heating through its influence on the magnetic fields (Skumanich 1972). Similarly, solar active regions are of course associated with regions of enhanced fields. The discussion of wave chromospheric heating is therefore incomplete without consideration of MHD modes which must be present along with pure acoustic modes. Osterbrock (1961) has shown that fast mode waves will steepen and shock in a very similar manner to that of the pure acoustic shocks discussed above, as long as the Alfvén speed A is $\leq a$. For moderate field strengths $\leq$ a few gauss, this condition is satisfied in the low chromospheres of all the models, so that we expect the basic chromospheric structures derived on the basis of pure acoustic modes to be representative of the results for magnetic shock heating. However, at larger heights and lower densities, a fast mode will change its character from that of an acoustic mode, so that the derived temperature structure will differ in the upper chromosphere.

III. WAVE-DRIVEN WINDS

a) Acoustic Waves

The observational evidence reviewed in § I indicates that the winds associated with low-gravity late-type stars are fundamentally different from the presumed thermally driven mass loss characteristic of dwarfs like the Sun. We have also noted that none of the proposed mechanisms for driving winds from these stars appear to be capable of accounting for their physical properties in a manner consistent with observation. The results of the previous sections, however, suggest that momentum deposition due to shock wave dissipation may be able to initiate mass loss in low-gravity stars, since the inclusion of this force in the hydrostatic calculations gave rise to extended chromospheric density distributions.

We have investigated this mechanism, and conclude that it is unlikely to lead to a continuous outflow of mass. Specifically, we find that shocks which result from the steepening of propagating waves with periods less than the acoustic cutoff period have dissipation lengths L typically $\sim$ a few scale heights. The distance L approximately characterizes the size of the region over which waves are effective in accelerating the flow, and is considerably smaller than the stellar radius R for all but the lowest gravity stars. As a result, the force due to shock dissipation is significant only in a narrow (thickness $\ll R$) zone of high-density gas near the base of the atmosphere, and becomes small before the flow has attained escape velocity. Thus it appears that the primary dynamical effect of propagating acoustic waves and the shocks that develop from them is to extend the essentially hydrostatic portions of the lower atmosphere, rather than to drive a steady stellar wind.

We note that the above conclusions do not, in general, apply to large-amplitude compressional disturbances which are not subject to period restrictions arising from the acoustic cutoff. In particular, propagating shocks generated by pulsation have been shown to produce mass ejection from low-gravity long period variable stars (Wood 1979; Willson and Hill 1979).

b) Alfvén Waves

Observations of large amplitude, outwardly propagating Alfvén waves in the solar wind (see, e.g., Belcher and Davis 1971) suggest that such modes may be present in the outer layers of late-type stars with mechanically heated chromospheres. In the case of the Sun, several authors (Belcher 1971; Alazraki and Couturier 1971; Hollweg 1973; Jacques 1977, 1978) have noted that these waves do work on the expanding solar corona, thereby modifying the dynamical structure of the solar wind. More importantly, it has been shown that undamped Alfvén waves can drive a wind from stars with atmospheres too cool to undergo thermally driven mass loss (Belcher 1971). These results motivate us to consider the effect of an Alfvén wave energy flux of magnitude comparable to solar values on the dynamics of winds from cool, low-gravity stars.

i) *Equations of Motion*

Following the treatment of Jacques (1977), we neglect stellar rotation and assume that the wind can be represented as a steady, radial flow. The magnetic field B is taken to be radially directed with strength $B=B_0(r_0/r)^2$, where r is the distance from the center of the star and r_0 is the location of a reference level in the stellar atmosphere (the subscript zero denotes evaluation at r_0). Under these conditions, conservation of mass yields an expression for the

(constant) mass loss rate

$$\dot{M}=4\pi r^2\rho u, \tag{28}$$

where ρ and u are, respectively, the mass density and wind velocity at r.

We consider small amplitude ($\delta B\ll B$), outwardly propagating Alfvénic fluctuations with wavelengths short compared with the scale lengths over which the physical properties of the wind vary. For waves with propagation vectors k parallel to u, the dispersion relation is given by $\omega=k(u+A)$, where ω is the (constant) wave frequency and $A=B(4\pi\rho)^{-1/2}$ is the Alfvén speed. In the solar wind, linear Alfvén waves of energy density $\epsilon=\delta B^2/8\pi$ are undamped, and the wave action density S, defined as

$$S=\frac{\epsilon}{\omega-ku}=\frac{\epsilon}{\omega}\frac{u+A}{A}, \tag{29}$$

is conserved (Jacques 1977). Unlike the solar case, however, the physical conditions in the expanding atmospheres of low-gravity stars suggest that propagating Alfvén waves can be appreciably damped. For example, the inferred cool temperatures ($T\leq 10^4$ K) of supergiant winds imply the presence of neutral gas which does not interact directly with the fluctuating magnetic field. As a result, linear Alfvénic disturbances are subject to dissipation arising from the friction between the ionized and neutral components of the outflowing material (see below). Characterizing this and other possible dissipation processes by a damping length L, the condition of wave action density conservation is replaced by (Jacques 1977)

$$\nabla\cdot(v_g S)=-v_g S/L, \tag{30}$$

where $v_g=\partial\omega/\partial\kappa=u+A$ is the group velocity of the waves. Equations (28) and (29), together with the assumption that u, B, and k are all radial, permit equation (30) to be rewritten in the form

$$\frac{d}{dr}\left[\epsilon M_A(1+M_A)^2\right]=-\frac{1}{L}\epsilon M_A(1+M_A)^2, \tag{31}$$

in which $M_A\equiv u/A$ is the Alfvénic Mach number. In deriving (31), we have made use of the fact that $M_A=M_{A0}(\rho_0/\rho)^{1/2}$, where M_{A0} and ρ_0 are the reference level values of the Mach number and density, respectively. Note that in the absence of dissipation ($L\rightarrow\infty$), equation (31) yields the well-known expression for the wave energy density in the WKB approximation, $\epsilon\propto[M_A(1+M_A)^2]^{-1}$ (Parker 1965; Belcher 1971; Jacques 1977).

With wave properties as described above, conservation of momentum for the outflowing gas take the form

$$u\frac{du}{dr}=-\frac{1}{\rho}\frac{dP}{dr}-\frac{GM}{r^2}-\frac{1}{2\rho}\frac{d\epsilon}{dr}, \tag{32}$$

where M is the stellar mass, P is the thermal pressure, and $f_W\equiv-\frac{1}{2}d\epsilon/dr$ is the time-averaged force per unit volume due to the waves. An explicit expression for f_W can be obtained from equation (31) by performing the indicated differentiation and using conservation of mass; the result is

$$f_w=-\frac{1}{2}\frac{d\epsilon}{dr}=\frac{\epsilon}{2L}+\frac{\epsilon}{4}\left(\frac{1+3M_A}{1+M_A}\right)\left(\frac{2}{r}+\frac{1}{u}\frac{du}{dr}\right). \tag{33}$$

Assuming a polytrope relation between P and ρ, i.e., $P\propto\rho^\gamma$ with γ the constant polytrope index, equations (32) and (33) can be combined to obtain the wind equation of motion

$$\left[u^2-a^2-\frac{\epsilon}{4\rho}\left(\frac{1+3M_A}{1+M_A}\right)\right]\frac{du}{dr}=\frac{2u}{r}\left[a^2-\frac{1}{2}\frac{GM}{r}+\frac{\epsilon}{4\rho}\left(\frac{1+3M_A}{1+M_A}\right)+\frac{\epsilon}{4\rho}\frac{r}{L}\right], \tag{34}$$

where $a=(\gamma P/\rho)^{1/2}$ is the sound speed.

ii) *Wind Solutions*

To illustrate the dynamical properties of winds driven by Alfvén waves, we have numerically integrated the equation of motion (34), assuming for simplicity that the outflow is isothermal ($\gamma=1$) and that the wave dissipation length is constant. The second of these assumptions enables us to obtain an expression for the wave energy density ϵ

TABLE 3

ALFVÉN-WAVE–DRIVEN WIND MODELS

No.	$M(M_\odot)$	$R(R_\odot)$	T(K)	N_0(cm^{-3})	$\mu(M_H)$	λ	B_0(G)	F_0(ergs cm^{-2} s^{-1})	$\dot{M}(M_\odot$ yr$^{-1})$	V_∞(km s^{-1})
1 ..	16	400	10^4	10^{11}	0.667	∞	1	3.36×10^3	1.09×10^{-10}	822.8
2 ..	16	400	10^4	10^{11}	0.667	∞	5	4.20×10^5	4.32×10^{-8}	508.1
3 ..	16	400	10^4	10^{11}	0.667	∞	10	3.36×10^6	5.47×10^{-7}	407.8
4 ..	16	400	10^4	10^{11}	0.667	1	1	3.36×10^3	5.83×10^{-11}	31.61
5 ..	16	400	10^4	10^{11}	0.667	1	5	4.20×10^5	3.14×10^{-8}	47.65
6 ..	16	400	10^4	10^{11}	0.667	1	10	3.36×10^6	4.51×10^{-7}	50.97
7 ..	16	400	5000	10^{11}	1.2754	1	1	2.43×10^3	2.23×10^{-11}	57.65
8 ..	16	400	5000	10^{11}	1.2754	1	5	3.04×10^5	1.32×10^{-8}	57.39
9 ..	16	400	5000	10^{11}	1.2754	1	10	2.43×10^6	2.02×10^{-7}	54.30
10 ..	16	400	5000	10^{12}	1.2754	1	1	7.68×10^2	2.29×10^{-12}	54.72
11 ..	16	400	5000	10^{12}	1.2754	1	5	9.60×10^4	1.38×10^{-9}	58.31
12 ..	16	400	5000	10^{12}	1.2754	1	10	7.68×10^5	2.15×10^{-8}	58.32
13 ..	16	1000	5000	10^{11}	1.2754	1	1	2.43×10^3	6.45×10^{-10}	28.53
14 ..	16	1000	5000	10^{11}	1.2754	1	5	3.04×10^5	3.57×10^{-7}	32.35
15 ..	16	1000	5000	10^{11}	1.2754	1	10	2.43×10^6	5.22×10^{-6}	32.49
16 ..	1.33	27	10^4	10^{11}	0.667	∞	10	3.36×10^6	1.77×10^{-9}	484.1
17 ..	1.33	27	10^4	10^{11}	0.667	1	10	3.36×10^6	1.46×10^{-9}	56.30
18 ..	1.33	27	5000	10^{11}	1.2754	1	10	2.43×10^6	6.67×10^{-10}	61.50
19 ..	1.33	10	5000	10^{11}	1.2754	1	10	2.43×10^6	2.03×10^{-11}	110.0
20 ..	10	1330	5000	10^{11}	1.2754	1	10	2.43×10^6	3.08×10^{-5}	22.5

by direct integration of equation (31), namely

$$\epsilon=\epsilon_0\frac{M_{A0}}{M_A}\left(\frac{1+M_{A0}}{1+M_A}\right)^2\exp\left[-\left(\frac{r-r_0}{L}\right)\right], \tag{35}$$

where, if δB_0 is the wave amplitude at $r=r_0$, $\epsilon_0=\delta B_0^2/8\pi$. Mass loss rates and terminal velocities (measured at $r=150\ R$) for wind solutions corresponding to a variety of values for the stellar surface gravity, reference level number density and magnetic field strength, gas temperature, and wave damping length are listed in Table 3. In all cases, the gas temperature is sufficiently low that in the absence of waves the thermally driven mass loss rate is negligible. Since the wind velocity at the reference level location (chosen to be $r_0=R$) is generally small compared with A_0, the initial Alfvén wave energy flux is

$$F_0=\frac{\delta B_0^2}{8\pi}A_0=1.12\times10^{-2}\alpha B_0^3\rho_0^{-1/2}\ \text{ergs cm}^{-2}\ \text{s}^{-1}, \tag{36}$$

with $\alpha=(\delta B_0/B_0)^2$. Adopting $\alpha=10^{-1}$ for each of the solutions listed in Table 3 results in values for $F_0\sim10^3$ to 10^6 ergs cm^{-2} s^{-1}, in reasonable agreement with the range of values suggested for the Sun (see Jacques 1978, and references contained therein).

The topology of solutions to this equation of motion is exceedingly complex. In the Appendix we present an analysis of the critical point behavior of model 6, which can be generalized to the other models with damping.

For a typical supergiant gravity ($M=16\ M_\odot$, $R=400\ R_\odot$), solutions 1 through 6 exemplify the effects of variations in the initial magnetic field strength B_0 for damped ($\lambda=L/R=1$) and undamped ($\lambda=\infty$) waves, assuming $T=10^4$ K. Since each solution is characterized by the same values for the initial number density ($N_0=10^{11}$ cm^{-3}), mean mass per particle ($\mu=0.667\ M_H$), and $\alpha(=10^{-1})$, varying B_0 is equivalent to varying the initial wave energy flux F_0. Note that in the absence of dissipation (solutions 1–3), increasing F_0 leads to higher initial velocities (and consequently, to larger values of $\dot{M}$) and lower terminal velocities, in agreement with the results of Belcher and Olbert (1975). However, since undamped Alfvén waves persist in the flow out to large distances from the star, they are capable of accelerating the gas in the low density portions of the wind ($r\approx10R$), resulting in terminal velocities which are unacceptably large in comparison with those inferred from observations. When wave dissipation is included (solutions 4–6), the mass loss rate $\dot{M}$ again increases with increasing F_0, attaining a value $\dot{M}\approx5\times10^{-7}\ M_\odot$ yr^{-1} for $F_0\approx3\times10^6$ ergs cm^{-2} s^{-1}. More importantly, depletion of the wave energy flux due to damping in the high density region of the flow within a stellar radius of the surface gives rise to terminal velocities an order of magnitude

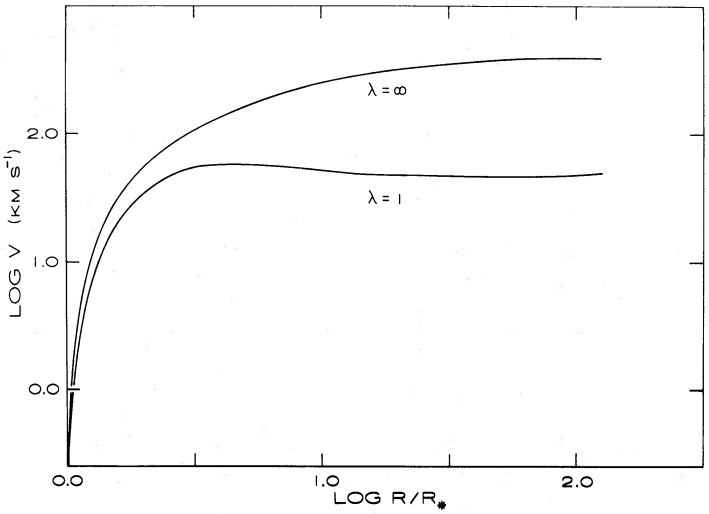

FIG. 5.—Velocity structures of Alfvén wave-driven winds. High terminal velocities occur for no wave dissipation (model 3 in Table 3); low wind speeds occur for damping lengths of a stellar radius ($\lambda = 1$, model 6).

or more below the corresponding solutions for undamped waves. Furthermore, examination of solutions 7–9 ($T = 5000$ K, $N_0 = 10^{11}$ cm^{-3}) and 10–13 ($T = 5000$ K, $N_0 = 10^{12}$ cm^{-3}) reveals that to within differences in the values of F_0, these results are relatively insensitive to changes in T and, to a lesser extent, to changes in N_0. Thus, for energy fluxes not unlike those suggested for the Sun, the force due to Alfvén waves can account for the magnitudes of both the mass loss rate and terminal velocities of supergiant winds, provided the waves are damped with a characteristic dissipation length of the order of the stellar radius.

For comparison, Figure 5 depicts the wind velocity profiles corresponding to solutions 3($\lambda = \infty$) and 6($\lambda = 1$) (see also Fig. 6). Many of the features of these profiles can be qualitatively understood by noting that, in each case, the force per unit mass due to Alfvén waves is a nonmonotonic function of distance from the surface of the star. In particular, near the base of the wind where u/a and u/A are both $\ll 1$, the wave force per unit mass is given by (cf. eq. [33])

$$\frac{f_w}{\rho} \approx \frac{\epsilon}{2\rho}\left(\frac{1}{L} - \frac{1}{2\rho}\frac{d\rho}{dr}\right) \approx \frac{\epsilon}{2\rho}\left(\frac{1}{L} + \frac{1}{2h}\right), \tag{37}$$

where the first term in parentheses is absent in the case of undamped waves ($L = \infty$). For $r \approx r_0$, the density distribution is close to hydrostatic, and the local scale height h (determined by the balance between the forces due to gravity, thermal pressure, and Alfvén waves) is considerably smaller than the stellar radius. From equation (35),

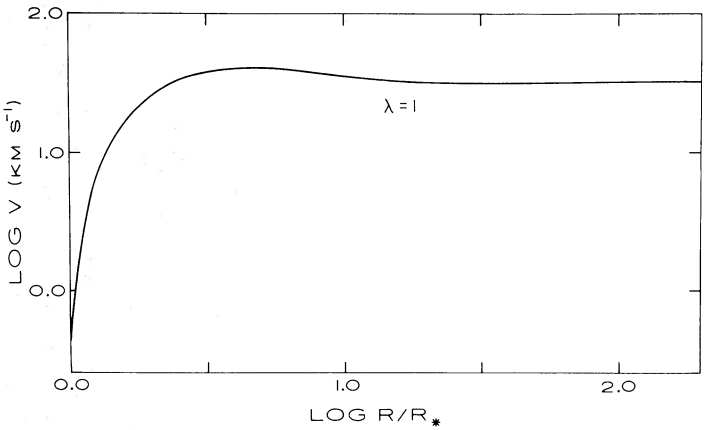

FIG. 6.—Velocity structure for model 17 in Table 3.

$\epsilon \approx \epsilon_0(M_{A0}/M_A) = \epsilon_0(\rho/\rho_0)^{1/2}$, so that f_w/ρ varies approximately as $\rho^{-1/2}$ and the wave force per unit mass increases outward from the surface of the star. Since $h \ll L$, the magnitude of f_w/ρ for r in the immediate vicinity of r_0 is nearly the same for solutions 3 and 6, and consequently both solutions have similar initial velocity profiles and mass loss rates.

At large distances ($r \gg R$), the flow in the case of undamped waves is characterized by $u \to u_\infty = \text{constant}$, $du/dr \to 0$, and $M_A \to \infty$. In this limit equations (33) and (35) imply that $\epsilon \approx \epsilon_0(M_{A0}/M_A^3) = (\epsilon_0/M_{A0}^2)(\rho/\rho_0)^{3/2}$ and $fw/\rho \approx (3\epsilon/2\rho r) \propto r^{-2}$. Thus, the magnitude of the wave force per unit mass approaches zero as $r \to \infty$, but its decrease is sufficiently gradual that the wind can still be accelerated at large distances from the star. In the specific case of solution 3, f_w/ρ is greater than either the gravitational or thermal pressure force at distances as large as the location of the Parker critical point ($r = GM/2a^2 \approx 31R$) appropriate to isothermal flow in the absence of waves.

When dissipation is included, the exponential decay of the wave energy density causes f_w/ρ to decrease rapidly in magnitude for distances $\geq L$. Thus, after an initial increase, f_w/ρ becomes smaller than the gravitational and thermal pressure forces within several stellar radii of the surface. The resulting peak in the wave force distribution gives rise to the presence of multiple critical points in the topology of solutions to the wind equation of motion (34), unlike the case of undamped waves for which a single critical point exists. For the present discussion, it is sufficient to note that the wind solution satisfying the boundary conditions of subsonic flow at $r = r_0$ and vanishing gas pressure at infinity passes smoothly through the first critical point. At larger distances, the flow continues to be accelerated until the wave flux is sufficiently depleted that the gas begins to be gravitationally decelerated. In the case of solution 6, the onset of gravitational deceleration occurs at $r \approx 4.6R$, where the sum of f_w/ρ and the thermal pressure force per unit mass ($\approx 2a^2/r$) first becomes smaller than GM/r^2. Deceleration of the gas continues until the location of the Parker critical point is attained ($r \approx 31R$), beyond which $2a^2/r > GM/r^2$ and the wind is thermally reaccelerated.

iii) *Alfvén Wave Dissipation*

The results of the preceding section indicate that the mass loss rate due to a wind driven by Alfvén waves is primarily determined by the initial wave energy flux F_0, while the terminal velocity is controlled by the damping length L. In view of the extent to which wave damping can affect the dynamical properties of the wind, we now enumerate some potential dissipation mechanisms for linear waves and, where possible, estimate the magnitudes of the associated damping lengths.

As noted previously, collisions between ions and neutral atoms cause small-amplitude Alfvén waves in a partially ionized gas to be damped by friction. For a gas consisting of a single ion species and a single species of neutral atoms, each characterized by a Maxwellian distribution function with the same temperature T, the neutral-ion collision time τ_{ni} is given by (Braginskii 1965)

$$\tau_{ni}^{-1} \approx \frac{2m_i N_i \sigma_{ni}}{m_i + m_n}\left(\frac{2kT}{\pi}\frac{m_i + m_n}{m_i m_n}\right)^{1/2}, \tag{38}$$

where m_i and m_n are, respectively, the ion and neutral particle masses, N_i is the ion number density, and σ_{ni} is the velocity-averaged collision cross section. When the plasma is composed of a single ion species and several types of neutral atoms, we confine our attention to waves having periods P_w such that $P_w \gg \tau_{ni}$ for each type of neutral partical present in the gas. Under these conditions, the average neutral-ion collision time $\bar{\tau}_{ni}$ can be defined as

$$\bar{\tau}_{ni}^{-1} = \sum_n (\rho_n/\tau_{ni}) / \sum_n \rho_n, \tag{39}$$

and the ionized and neutral components of the gas move together in the wave ($\delta V_i \approx \delta V_n$). Moreover, the phase speed of a wave propagating in the direction of the ambient magnetic field is the Alfvén speed calculated using the total mass density of the gas,

$$\rho = \rho_i + \sum_n \rho_n,$$

and the dissipative effect of ion-neutral friction causes the wave energy density to decrease by a factor of e in a distance L_F given by

$$L_F = \frac{AP_w^2}{4\pi^2 \bar{\tau}_{ni}}\frac{1+\xi}{\xi}, \tag{40}$$

where

$$\xi \equiv \sum_n \rho_n / \rho_i$$

(Piddington 1956; Osterbrock 1961; Kulsrud and Pierce 1969).

To obtain an estimate of the frictional damping length for Alfvén waves in late-type stellar winds, we adopt physical conditions ($N = 10^{11}$ cm^{-3}, $T = 5000$ K, $B = 10$ gauss) representative of those at the base ($r \approx R$) of a supergiant wind (solution 9 of Table 3), where shock wave dissipation is expected to be the dominant heating mechanism and the density distribution is nearly hydrostatic. For simplicity, we assume that the gas is composed of hydrogen and helium $N = N_{\rm H} + N_{\rm He} + N_e$, where helium is taken to be completely neutral and the electron number density is due to hydrogen ionization. The presence of singly ionized metals has been neglected because, for the assumed conditions of temperature and density, metal ions are less abundant than protons and the neutral-metal collision time is correspondingly greater than the time for neutral-proton collisions. Application of the ionization analysis of § II*b* for $N_{\rm He}/N_{\rm H} = 0.10$ and $A_m = 0$ yields $N_e = N_{\rm H\ II} = 2.18 \times 10^8$ cm^{-3}, $N_{\rm H\ I} = 9.05 \times 10^{10}$ cm^{-3}, and $N_{\rm He} = 9.07 \times 10^9$ cm^{-3}. The frictional damping of Alfvén waves is due to collisions of neutral hydrogen and helium atoms with protons, for which approximate cross section values are $\sigma({\rm H}, {\rm H}^+) \approx 5 \times 10^{-15}$ cm^2 and $\sigma({\rm He}, {\rm H}^+) \approx 8 \times 10^{-16}$ cm^2, respectively (Osterbrock 1961). From equations (38) and (39), the individual collision times associated with these processes are $\tau({\rm H}, {\rm H}^+) \approx 1.27$ s and $\tau({\rm He}, {\rm H}^+) \approx 25.03$ s, and the average neutral-ion collision time in the gas is $\bar{\tau}_{ni} \approx 1.74$ s. With $\xi = (\rho_{\rm H\ I} + \rho_{\rm He})/\rho_{\rm H\ II}$ and the previously adopted magnetic field strength, the resulting value for the frictional damping length is

$$L_F \approx 8.93 \times 10^4 P_w^2 \text{ cm}. \tag{41}$$

Thus, $L_F \approx R$ for a wave with period $P_w \approx 1.77 \times 10^4$ s, a value sufficiently long to ensure that $P_w \gg \tau({\rm H}, {\rm H}^+)$, $\tau({\rm He}, {\rm H}^+)$.

Small-amplitude Alfvén waves propagating through a partially ionized gas also dissipate energy by Joule heating (an effect arising from the finite conductivity of the plasma) and by the effects of viscosity (due primarily to ion collisions in the plasma). However, we find that the damping lengths due to these processes are very much longer than the typical frictional damping length, and thus are unimportant.

In addition to the mechanisms discussed above, Alfvén wave dissipation can also occur via mode conversion and nonlinear wave-wave interactions. Each of these processes is characterized by the conversion of a fraction of the Alfvén wave energy into a propagating compressional disturbance which is subsequently damped. For example, an Alfvén wave traveling through a region of inhomogeneous magnetic field will be partially transformed into a fast-mode wave if the field bends in the direction of the Alfvénic velocity fluctuation δV (Wentzel 1974). Although our models assume for simplicity that the magnetic field is radially directed, comparison with the solar case suggests that in reality the field near base of the flow may exhibit appreciable curvature. As a result, some conversion of Alfvén waves to fast mode waves must take place over a distance comparable to the field radius of curvature, so that if the magnetic field curves on a typical scale of a stellar radius, it is possible to arrive at dynamically satisfactory values of the damping length L. In the absence of a specific model for the field geometry and distribution of wave vector directions, we cannot calculate the efficiency of this process. Similarly, several authors (Sagdeev and Galeev 1969; Chin and Wentzel 1972; Wentzel 1974) have shown that when $A > a$, an Alfvén wave propagating parallel to the background magnetic field can decay into a sound wave traveling in the same direction and an oppositely propagating Alfvén wave (provided some amplitude of the resulting waves exists prior to the decay to initiate the interaction). As before, we note that while such processes probably contribute to, and could well dominate, the wave dissipation near the base of the wind, the assumptions inherent in our treatment of wave propagation prohibit us from calculating the effective damping length.

We conclude this section by considering the dissipation of Alfvén waves by frictional damping at large distances from the surface of the star. Toward this end, we evaluate the frictional damping length at $r \approx 2R$ in the model supergiant wind given by solution 9. At this point in the flow, $u \approx 44$ km s^{-1}, $N_{\rm H} \approx 3.06 \times 10^7$ cm^{-3}, $B \approx 2.43$ gauss and the wave energy flux has decreased from its reference level value to $F \approx 1.90 \times 10^5$ ergs cm^{-2} s^{-1}. Assuming $T = 5000$ K, the hydrogen ionization equilibrium and neutral-ion collision times can be calculated according to the procedure described above. The lower density at $r = 2R$ causes $\bar{\tau}_{ni}$ to increase by a factor $\sim 10^2$, leading to a larger phase lag between the ion and neutral motions and an enhanced wave dissipation rate. Consequently, for a wave with period $P_w \approx 1.77 \times 10^4$ s having $L_F \approx R$ at the base of the wind, the frictional damping length at $r = 2R$ has decreased to a value $L_F \approx 0.087R$. We note, however, that the local heating rate due to Alfvén wave dissipation implied by these results is approximately $F/L_F \approx 7.83 \times 10^{-8}$ ergs cm^{-3} s^{-1}, a value several orders of magnitude in

excess of the local radiative cooling rate for $T \approx 5000$ K, estimated using the cooling coefficient of Table 1. We therefore conclude that the gas temperature at $r = 2R$ must be greater than the assumed value.

An approximate determination of the temperature at this distance can be obtained by assuming that the gas is sufficiently hot that hydrogen is essentially fully ionized, but that helium remains neutral. In this case, $N_{\rm H} \approx N_{\rm H\,II} = N_e \approx 3.06 \times 10^7$ cm^{-3} and $\bar{\tau}_{ni} \approx \tau({\rm He}, {\rm H}^+) \approx 1.26 \times 10^4 / T^{1/2}$ s. With $\xi = \rho_{\rm He}/\rho_{\rm H\,II}$, the frictional damping length is (cf. eq. [40]) $L_F \approx 5.69 \times 10^2 T^{1/2} P_w^2$ cm, so that, for a given wave period, the heating rate F/L_F is a function only of T. Using the values of the solar cooling coefficient listed in Table 1 to estimate the radiative losses, the thermal balance equation $F/L_F \approx N_e^2 P_R(T)$ (neglecting the effects of heat conduction and adiabatic cooling, which are both small) can now be solved for the equilibrium gas temperature T. For a wave of period $P_w \approx 1.77 \times 10^4$ s, we find $T \approx 13{,}300$ K with $L_F \approx R$ at $r = 2R$. Thus, if the force due to long-period Alfvén waves is responsible for mass loss from late-type low-gravity stars, the frictional dissipation of these modes should give rise to the presence of warm ($T \sim 10^4$ K) gas within several stellar radii of the surface. Note that it is unlikely that a flux of acoustic waves of magnitude sufficient to account for such heating could survive to these distances in the wind because of their short damping lengths.

Finally, we point out that the existence of a temperature increase at larger distances should not result in significant modifications to the dynamical properties of the calculated isothermal wind model. Since the heating rate due to Alfvén wave dissipation is small in comparison with the radiative cooling rate at $T = 5000$ K for densities characteristic of $r \approx R$, the mass loss rate corresponding to the model should not be affected. Furthermore, because the initial acceleration of the wind is due almost entirely to the wave force, the wind properties are relatively insensitive to changes in the gas temperature, provided such changes do not lead to substantial variations in the damping length. In this regard, we note that the temperature of the outflow is in fact limited by the behavior of the damping length. At a temperature sufficiently high that helium becomes appreciably ionized, the frictional damping length will increase in magnitude, thereby reducing the wave heating rate and lowering the temperature.

iv) *Temperature Structure of Winds and the Transition from Coronal to Cool Mass Loss*

In the previous section we showed that there are several mechanisms by which Alfvén waves may be expected to dissipate. We are unable to predict the damping length even in the case of frictional dissipation for lack of knowledge of the wave period. However, if we regard F_o and L as set by observations of the mass loss rate and terminal velocity, respectively, then the heating rate F_o/L is fixed. An estimate of the cooling rate then yields the temperature, for radiative cooling and wave heating dominate the energy balance through the equation

$$F/L \sim \Lambda_R(T) N_{\rm H} N_e. \tag{42}$$

We find that the other terms in the energy equation, involving the wind expansion, are small when compared with the radiative cooling term.

In order for the models to be self-consistent, the thermal pressure gradient must be unimportant; in effect this means that the gas temperature must be $\ll 10^5$ K. The heating implied by F/L for model 20, intended to represent α Ori, results in a temperature $\sim 5 \times 10^3$ K, extending over a region of ~ 5 stellar radii. We caution that the temperature determination is very approximate from the uncertainties in the cooling law and ionization balance. The wind temperature rises with increasing stellar gravity, principally because the wind density drops. Model 18, with $\log g = 1.7$ has a temperature $\sim 2 \times 10^4$ K at the critical point and a temperature range $\sim 20{,}000$–$30{,}000$ K from about 1.1 R_* to about 7 R_*. This still indicates little thermal expansion.

However, the wave heating in model 19, with $\log g = 2.56$, implies temperatures in excess of 10^5 K near the critical point. Therefore model 19 is *not* self-consistent. We infer that low-velocity winds cannot be generated by Alfvén wave pressure for $\log g \gtrsim 2$. Wave dissipation at high gravity results in thermal expansion and coronal winds. If no dissipation occurs, the wind speeds are too high.

This result is compatible with observations, which indicate a transition in wind behavior near $\log g \sim 2$ from coronal winds to cool, low-velocity flows (Reimers 1977*a*; Mullan 1978; Linsky and Haisch 1979). The exact value of $\log g$ at which the transition occurs will depend on the details of dissipation and on the exact amount of wave flux available.

Models of the solar corona require mechanical energy fluxes $\sim 10^5$–10^6 ergs cm^{-2} s^{-1} in order to balance radiative losses (Rosner and Vaiana 1978). A similar flux of energy appears to be required for mass loss; wave dissipation will result in coronae (with L assumed to be of the order of the stellar radius) for $\log g \gtrsim 2$ as required by observation. This suggests that the same mechanism, dissipation of Alfvén waves, accounts for coronae in high-gravity stars, as well as for extended chromospheres and mass loss in low-gravity stars.

At this point we may comment on the relationship of the Haisch, Linsky, and Basri (1980) (HLB) model for Arcturus to our models. In general we have much different temperature and density structures than assumed in HLB, and it is not clear how dependent the HLB results are on the assumed chromospheric structure. For example, our supergiant models never achieve temperatures greater than ~10,000 K, in contrast to the 20,000 K plateau assumed in the HLB model. Even in model 18, representative of Arcturus, our heating calculations indicate that $T = 20{,}000$ K is formed at a much larger distance from the star ($r > 1.1\ R_*$) than in the HLB model. At this distance the flow is already expanding at a few km s^{-1} from the effects of the Alfvén wave force, indicating that the Alfvén waves are dominating the flow before the $L\alpha$ pressure becomes appreciable. It is hard for us to see how a force which contributes $\sim 3 \times 10^{-4}$ of the momentum deposition of the Alfvén waves can control the nature of the wind solution. In this connection we point out that HLB have not formally integrated through critical points, as they do not conserve mass to better than a factor of 4. In any event our low-gravity models will have such low temperatures that the $L\alpha$ line will become optically thin far out in the wind; since HLB indicate that the $L\alpha$ force is appreciable only at small line optical depths, we expect that this force will not become important interior to the critical point as in the HLB models.

v) *Predictions of Extended Chromospheres and Magnetic Fields*

Studies of chromospheric gas near the stellar surface are difficult to pursue in terms of the usual optical circumstellar shell lines. Models of such shells are parametrized by inner shell radii at large distances from the surface (cf. Bernat 1977); the inner physical conditions are not well understood. Weymann (1962) has suggested that α Ori has an extended warm chromosphere, based on the anomalous strength of Hα. Some chromospheric lines appear to be far from the surface, based on the fact that they do not follow the radial velocity pulsations of the primary (Goldberg 1979).

Recently Altenhoff, Oster, and Wendker (1979) have interpreted the radio emission of α Ori at frequencies below 20 GHz as rising from an extended photosphere-chromosphere region extending to about two or three stellar radii (see also Bowers and Kundu 1979). Further radio measurements, including angular diameter determinations, will be fruitful in identifying the extended chromospheres predicted by wave dissipation. The measured brightness temperatures are predicted to be ~5000 K over a distance of a few stellar radii, based on our model 20.

Other promising objectes for study are the ξ Aur binary systems, where the early-type companion may be used to probe the chromosphere of the primary. In their classic study of ξ Aur, Wilson and Abt (1954) found generally increasing excitation temperatures with increasing height. The primary of ξ Aur has $M \approx 22\ M_\odot$, $R \approx 200\ R_\odot$, so that our supergiant results are well suited for comparison. We pursue the following discussion in units of the scale height h, which compensates for the different gravities of ξ Aur and our supergiant model. Wilson and Abt (1954) found that the excitation temperatures ranged from ~4000 K to ~7000 K over a distance corresponding to $\sim 140\ h \approx 0.30\ R_*$. The corresponding density at 4000 K was found to be $\sim 10^{11}$ cm^{-3}, with a density scale height $\sim 7h$ increasing to $\sim 35h$ at the largest observed heights. The large observed scale heights suggest that a wind is causing departures from hydrostatic equilibrium for $N \leq 10^{11}$ cm^{-3}, in agreement with our models.

The derived values of excitation temperature are in qualitative agreement with what one would expect for Alfvén waves dissipation. Acoustic wave heating is unlikely to maintain these temperatures at ~80 scale heights from the temperature minimum. However, the analysis is not simple. Wilson and Abt conclude that the B star dominates the ionization balance, even though it cannot ionize the chromosphere appreciably through the Lyman continuum emission. They derive electron densities of the same order of magnitude as the neutral hydrogen density, which indicates substantial hydrogen ionization and temperatures ≥ 7000 K. This analysis is very uncertain; the electron densities are derived indirectly through an approximate ionization balance equation. The result requires pockets or clouds of material $\sim 10^2$ denser than the surrounding gas, which may be questionable. We expect that direct ultraviolet observations, such as the *IUE* study of VV Cep by Hagen *et al.* (1980), will specify the ionization balance and excitation of temperatures more clearly, and permit a separation of the effects of the radiation field of the early-type companion from the intrinsic chromospheric excitation. At present the most that can be said is that the observations are compatible with the notion of wave heating in an extended chromosphere.

Reimers (1975) has inferred the presence of an inner Ca III zone extending outward a few stellar radii in M giants, based on the observed circumstellar line strength–radial velocity relation for different spectral types and for stars with variable CS lines. Reimers attributes this second ionization of Ca to photoionization by chromospheric radiation. However, it may also be due to heating from the dissipation of wave energy envisaged here. The hypothesis of photoionization should be reexamined in the light of *IUE* observations of ultraviolet fluxes.

Another important assumption of this theory is that stellar magnetic field strengths of a few gauss are present, in order to obtain reasonable mass loss rates. Reid *et al.* (1979) have observed circular polarization in the circumstellar maser emission of the Mira variable U Ori. The magnetic field inferred from these observations is ~10 milligauss, which, when extrapolated back to the stellar surface using a scaling of r^{-2}, implies a surface magnetic field

$\sim$10 gauss. Thus there is evidence for magnetic fields of the order assumed in these calculations on at least one late-type, luminous star.

It should be emphasized that the lowest-gravity stars, such as Mira variables, may well have winds which are strongly modified or even produced by pulsation and radiation pressure on grains rather than Alfvén waves. Our primary interest is in explaining the mass loss from the majority of late-type, luminous stars for which such mechanisms are not important.

vi) *General Behavior of Winds in the H-R Diagram*

The properties of the solutions listed in Table 3 permit some general comments to be made on the expected behavior of winds with constant surface magnetic fields and energy fluxes for various gravities. For magnetic fields $\approx$5–10 gauss we find mass loss rates which are generally within observational estimates. Although the details of dissipation, which we cannot describe at this point, determine the terminal velocity, for $\lambda \geq 1$ the mass loss rate is not greatly affected, so we may make predictions for the behavior of mass loss rates in the H-R diagram. (For $\lambda \ll 1$, mass loss ceases in these models). Goldberg (1979) has shown that several possible scaling laws for mass loss are equally compatible with the data; one very simple law is $\dot{M} = 2.6 \times 10^{-12} R^2 M_\odot$ yr^{-1}, where R is given in solar units. Using models 6, 15, and 17 from Table 3, we obtain an approximate relation $\dot{M} \sim 7.6 \times 10^{-13} R^{2.24} M_\odot$ yr^{-1}, in rough agreement with the aforementioned empirical law. We have not chosen to pursue this question further because of the very large uncertainties in empirical mass loss rates (Bernat 1977).

The variation of terminal velocities remains an open question. For a constant value of λ, the terminal velocity decreases with decreasing gravity, in agreement with observations. A damping length which scales with the stellar radius might arise from a suitable variation of wave periods, or possibly through the scaling of the magnetic field curvature. Observations of the inner wind temperature structure could yield estimates of the dissipation length without requiring a detailed understanding of the damping mechanism.

IV. CONCLUSIONS

We have shown that it is possible to understand the magnitude of mass loss from luminous late-type stars if it is assumed that they possess Alfvén wave surface fluxes of the same order of magnitude as the Sun. The main uncertainty in this theory is the predicted terminal velocity, which is a sensitive function of the detailed wave damping mechanisms which operate at the base of the wind and of the (unknown) wave periods. Coronal heating and low-velocity mass loss may result from the changing atmospheric response as a function of gravity to the same basic energy deposition mechanism. Observational searches for extended, warm chromospheres around late type supergiants have been suggested to test the theory.

We would like to acknowledge useful conversations with I. Lerche, E. Parker, R. Rosner, and E. Avrett. This work was supported in part by NASA grants NGL 14-001-001 to the University of Chicago and NSG 5370 to the Harvard College Observatory.

APPENDIX

CRITICAL POINT BEHAVIOR OF SOLUTIONS TO THE WIND EQUATION OF MOTION

In § III, it was noted that when the effect of Alfvén wave dissipation is included in the momentum equation for the wind, the wave force per unit mass f_w/ρ is a nonmonotonic function of distance from the surface of the star. In particular, if the waves are damped with a constant damping length L, then f_w/ρ is an increasing function of distance for $(r-R) \ll L$, a decreasing function for $(r-R) \geq L$, and becomes smaller than either the gravitational or thermal pressure force within several damping lengths from the base of the wind. Such a peak in the rate of momentum addition to the gas can lead to the existence of several critical points in the flow (Holzer 1977). In this appendix, we isolate the parameters upon which solutions to the isothermal wind equation depend, and determine the critical point locations when these parameters have a particular set of fixed values. From these results, we deduce the behavior of solutions in the vicinity of the critical points.

Adopting $r_0 = R$ as the reference level location, we define the scaled variables z and w by $z \equiv r/R$, $w \equiv u/a$. Using equation (35) for the wave energy density ϵ, the wind equation of motion (34) can be written in the form

$$\frac{dw}{dz} = \frac{2w}{z} \frac{N(w,z)}{D(w,z)}, \tag{A1}$$

where (in the notation of § III) the functions $N(w, z)$ and $D(w, z)$ are given by

$$N(w,z)=1-\frac{\xi}{2z}+\frac{\alpha M_A}{(1+M_A)^2}\left[\left(\frac{1+3M_A}{1+M_A}\right)+\frac{z}{\lambda}\right]\exp[-(z-1)/\lambda], \tag{A2}$$

$$D(w,z)=\left(\frac{M_A}{\beta z}\right)^4-1-\frac{\alpha M_A(1+3M_A)}{(1+M_A)^3}\exp[-(z-1)/\lambda], \tag{A3}$$

with $\lambda=L/R$, $\xi=(GM/a^2R)$, $\beta=aw_0^{1/2}/A_0$, and

$$\alpha=\frac{\epsilon_0}{4\rho_0 a^2}\frac{(1+M_{A0})^2}{M_{A0}}. \tag{A4}$$

For radially directed flows and magnetic field, the Alfvénic Mach number M_A is a function of w and z through the relation $M_A=\beta z w^{1/2}$. Following Lerche and Vasyliunas (1976), we seek the curves $w(z)$ along which $N(w, z)=0$ and $D(w, z)=0$, for fixed values of the parameters α, β, ξ, and λ. For purposes of illustration, we choose the specific values $\alpha=233.56$, $\beta=2.02\times10^{-2}$, $\xi=61.62$, and $\lambda=1$, appropriate to solution 6 of Table 3. The intersection points of the curves so derived will correspond to the locations of critical points in the (w, z) plane where N and D simultaneously vanish and dw/dz as given by equation (A1) is indeterminate.

We note that at a given location z, the equation represented by $N(w, z)=0$ is a cubic to be solved for M_A (cf. eq. [A2]). For the assumed values of α, β, ξ, and λ, $N(w, z)=0$ possesses three real roots M_A for $z<5.59$, of which one is negative and can be omitted from further consideration. The two remaining roots are both positive, and have the property that throughout most of the region $1\le z<5.59$, one root is much smaller than 1 ($M_A\ll1$), while the other is large ($M_A\gg1$). Approximate expressions for $w(z)$ corresponding to these roots are

$$w(z)\approx\left[\frac{1}{\alpha\beta z}\frac{(\xi/2z-1)}{(1+z/\lambda)}\exp[(z-1)/\lambda]\right]^2 \tag{A5}$$

for $M_A\ll1$, and

$$w(z)\approx\left[\frac{\alpha}{\beta z}\frac{(3+z/\lambda)}{(\xi/2z-1)}\exp[-(z-1)/\lambda]\right]^2 \tag{A6}$$

for $M_A\gg1$. At the point $z=5.59$, the two positive roots merge; for larger values of z, real roots greater than 0 to the equation $N(w, z)=0$ exist only for z in the narrow region $\frac{1}{2}\xi(1-\epsilon)\le z\le\xi/2$, where $\epsilon\ll1$. Examination of equation (A2) reveals that for z in this region, the set of solutions to $N(w, z)=0$ contains all values of M_A in the range $0\le M_A\le\infty$.

The equation $D(w, z)=0$ at a fixed position z is a polynomial equation of order seven to be solved for M_A (cf. eq. [A3]). For the assumed parameter values, it can be easily shown that $D(w, z)=0$ has a single real positive root M_A for all $z\ge1$. Near the base of the wind ($z\approx1$), the root is such that $M_A\ll1$, and the solution $w(z)$ can be given in approximate form as

$$w(z)\approx\{\alpha\beta z\exp[-(z-1)/\lambda]\}^{2/3}. \tag{A7}$$

At larger distances, the inclusion of wave damping causes the third term in equation (A3) to diminish in magnitude relative to each of the first two terms. As a result, the solution at large z approaches $M_A\approx\beta z$ or $w\approx1$.

The calculated lines $w(z)$ for which $N(w, z)=0$ and $D(w, z)=0$ are shown in Figure 7, along with the velocity profile corresponding to solution 6. The existence of three critical points in the (w, z)-plane is indicated from the presence of three intersections of the $N=0$ and $D=0$ curves. For the specified values of α, β, ξ, and λ, the intersections occur at the locations (w_c, z_c) given by (2.70, 1.78), (1.88, 3.03), and (1.00, 30.81), respectively. We note that the desired wind solution (i.e., that solution satisfying the boundary conditions of subsonic flow at $r=R$ and vanishing gas pressure at infinity) passes through the critical point closest to the surface of the star.

To ascertain the nature of solutions in the immediate vicinity of a critical point (w_c, z_c) we express the variables w and z in the form $w=w_c+\Delta w$, $z=z_c+\Delta z$ with $\Delta w\ll w_c$, $\Delta z\ll z_c$, and substitute in the equation of motion (A1).

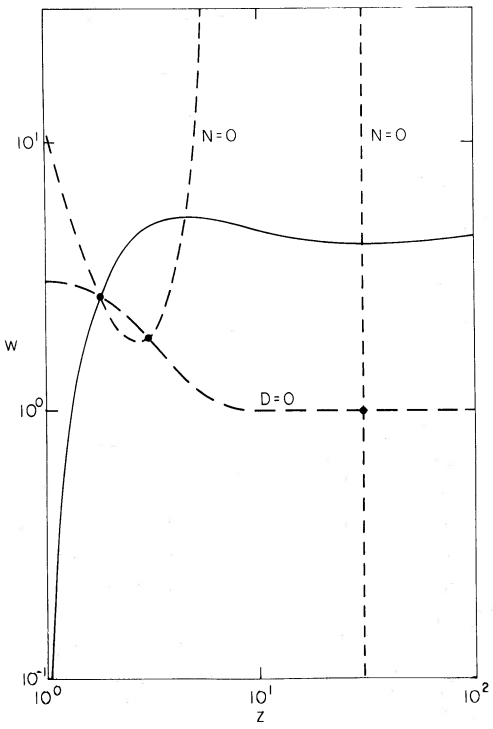

FIG. 7.—The curves $w(z)$ corresponding to $N=0$, $D=0$, and the critical velocity profile for the wind of model 6 (see Appendix). Critical point locations are indicated by heavy dots.

Expanding N and D about (w_c, z_c) and retaining only the terms which are linear in Δw and Δz, we obtain

$$\frac{d\Delta w}{d\Delta z} = \frac{C_1 \Delta w + C_2 \Delta z}{C_3 \Delta w + C_4 \Delta z}, \tag{A8}$$

where the constant coefficients C_1, C_2, C_3, and C_4 are proportional to the partial derivatives of N and D with respect to w and z evaluated at (w_c, z_c); specifically,

$$(C_1, C_2, C_3, C_4) = \left(2w\frac{\partial N}{\partial w}, 2w\frac{\partial N}{\partial z}, z\frac{\partial D}{\partial w}, z\frac{\partial D}{\partial z}\right)(w_c, z_c). \tag{A9}$$

We first consider the existence of solutions which pass through a given critical point with constant slope. Assuming $\Delta w = S\Delta z$ with S = constant, equation (A8) yields two values S_1, S_2 for the slope at each critical point,

$$S_{1,2} = \frac{1}{2}\left(\frac{C_1 - C_4}{C_3}\right) \pm \frac{1}{2}\left[\left(\frac{C_1 - C_4}{C_3}\right)^2 + 4\frac{C_2}{C_3}\right]^{1/2}, \tag{A10}$$

in which the subscript 1(2) corresponds to the $+(-)$ sign. The coefficients appearing in equation (A8) can be calculated by direct differentiation of equations (A2) and (A3), and evaluated at each of the locations (w_c, z_c) given above. When these values are inserted into equation (A10) for the solution slopes, the following results are obtained. At $(w_c, z_c) = (2.70, 1.78)$, the coefficients C_1, C_2, C_3, C_4 are all greater than 0, and S_1, S_2 have opposite signs and unequal magnitudes. Solutions of the form $\Delta w = S\Delta z$ therefore exist, and the critical point is a saddle point or X-type critical point. At $(w_c, z_c) = (1.88, 3.03)$, $C_1, C_3, C_4 > 0$ while $C_2 < 0$, and the values computed for S_1, S_2 are complex. In this case, there are no solutions of the assumed form that cross the critical point, indicating that the critical point is a focus or spiral point. At $(w_c, z_c) = (1.00, 30.81)$, $C_1 = C_4 = 0$ with $C_2, C_3 > 0$, so that S_1, S_2 are again real and of opposite sign, but now have equal magnitudes. This critical point is essentially the familiar X-type singularity

associated with the transonic flow of an isothermal wind, (see, e.g., Parker 1963), and occurs at the location $(w_c, z_c)=(1, \xi/2)$.

The form of the solution curves in the neighborhood of a critical point can be derived by assuming that Δw is expressible as $\Delta w=\mu\Delta z$ where μ is taken to be a function of Δz. With this substitution, equation (A8) can be integrated to obtain a relation between Δw and Δz of the form (cf. Lerche and Vasyliunas 1976).

$$(\Delta w-S_1\Delta z)^{-(S_1+C_4/C_3)}(\Delta w-S_2\Delta z)^{(S_2+C_4/C_3)}=\text{constant}, \tag{A11}$$

where the slopes S_1, S_2 and coefficients C_3, C_4 have been defined above. Using the previously determined values of these quantities, we find the following behavior for solutions near each of the three critical point locations. At the inner critical point, the solution curves are similar to hyperbolae, and are asymptotic to the lines $\Delta w=S_1\Delta z$ and $\Delta w=S_2\Delta z$, i.e, to the two critical solutions. At the middle critical point, all solution curves spiral toward the critical point in a counterclockwise sense. At the outer critical point, the solution curves constitute a family of hyperbolae, with the two critical solutions as asymptotes. We note that the same conclusions concerning the solution topology can be reached by attempting to sketch the curves $w(z)$ for solutions other than the wind solution shown in Figure 7. Given the positions of the $N=0$ and $D=0$ lines in Figure 7, this can be done by noting that a particular curve is vertical when crossing the $D=0$ line, horizontal when crossing the $N=0$ line, and that points on these lines are the only locations at which the slope of a curve can change sign.

While the quantitative results described in this section pertain only to the case of model 6 (for which the parameters α, β, ξ, and λ have the particular values assumed above), the critical point characteristics obtained from a similar analysis of the other $\lambda=1$ models (cf. Table 3) are qualitatively the same. For those wind models that do not include the effects of wave damping, only a single X-type critical point exists (see, e.g., Jacques 1977). This can be seen from equations (A2) and (A3) by holding α, β, and ξ at the values appropriate to model 6 and taking the limit $\lambda\to\infty$. In this case, the inner curve $w(z)$ for which $N=0$ (cf. Fig. 7) is a monotonically decreasing function of distance that crosses the z-axis at $z=\xi/2$, while the outer $N=0$ curve is absent. The shape of the $D=0$ curve is qualitatively the same as that shown in the figure, with the result that a single intersection of the $N=0$ and $D=0$ curves occurs; the location of this intersection is near that of the inner critical point in Fig. 7. We note also that a single critical point exists for the case in which $\lambda\to 0$. As λ is decreased with α, β, and ξ held fixed, the initial decrease in the $D=0$ curve moves closer to $z=1$, while the minimum of the $N=0$ curve shifts inward and increases in value. Thus, for $\lambda<\lambda_c$, where the value of λ_c depends upon λ, β, and ξ, the $N=0$ and $D=0$ curves intersect only at $(w_c, z_c)=(1, \xi/2)$, and a single critical point exists. For parameter values characteristic of model 6, this transition occurs for $\lambda<\lambda_c\approx 0.9$.

REFERENCES

Alazraki, G., and Couturier, P. 1971, *Astr. Ap.*, **13**, 380.
Altenhoff, W. J., Oster, L., and Wendker, H. J. 1979, *Astr. Ap.*, **73**, L21.
Ayres, T. R. 1975, Ph.D. thesis, University of Colorado.
_____. 1979, *Ap. J.*, **228**, 509.
Ayres, T. R., Linsky, J. L., and Shine, R. 1975, *Ap. J. (Letters)*, **195**, L121.
Baliunas, S. L., Avrett, E. A., Hartmann, L., and Dupree, A. K. 1979, *Ap. J. (Letters)*, **233**, L129.
Basri, G. S. 1979, Ph.D. thesis, University of Colorado.
Belcher, J. W. 1971, *Ap. J.*, **168**, 509.
Belcher, J. W., and Davis, R. L. 1971, *J. Geophys. Res.*, **76**, 3534.
Belcher, J. W., and Olbert, S. 1975, *Ap. J.*, **200**, 369.
Bernat, A. P. 1977, *Ap. J.*, **213**, 756.
Bowers, P. F., and Kundu, M. R. 1979, *A. J.*, **84**, 791.
Braginskii, S. I. 1965, in *Reviews of Plasma Physics*, Vol. **1**, ed. M. A. Leontovich (New York: Consultants Bureau).
Chin, Y., and Wentzel, D. G. 1972, *Ap. Space Sci.*, **16**, 465.
Chiu, H. Y., Adams, P. S., Linsky, J. L., Basri, G. S., Maran, S. P., and Hobbs, R. W. 1977, *Ap. J.*, **211**, 453.
de Loore, C. 1968, *Ap. Space Sci.*, **6**, 60.
Deutsch, A. J. 1956, *Ap. J.*, **123**, 210.
_____. 1960, in *Stellar Atmospheres*, ed. J. C. Greenstein (Chicago: University of Chicago Press), p. 543.
Dupree, A. K. 1976, in *Physique des Mouvements dans les Atmospheres Stellaires*, ed. R. Cayrel and M. Steinberg (CNRS), p. 439.
Gehrz, R. D., and Woolf, N. J. 1971, *Ap. J.*, **165**, 285.
Gingerich, O. 1964, Smithsonian Ap. Obs. Special Report 167, 17.
Giovanelli, R. G. 1978, *Solar Phys.*, **59**, 293.
Goldberg, L. 1979, *Quart. J.R.A.S.*, **20**, 361.
Hagen, W. 1978, *Ap. J. Suppl.*, **38**, 1.
Hagen, W., Black, J., Dupree, A. K., and Holm, A. V. 1980, *Ap. J.* in press.
Haisch, B. M., Linsky, J. L., and Basri, G. 1980, *Ap. J.*, **235**, 519 (HLB).
Hartmann, L., Dupree, A. K., and Raymond, J. C. 1980, *Ap. J. (Letters)*, **236**, L143.
Hollweg, J. V. 1973, *Ap. J.*, **181**, 547.
Holzer, T. E. 1977, *J. Geophys. Res.*, **82**, 23.
Jacques, S. A. 1977, *Ap. J.*, **215**, 942.
_____. 1978, *Ap. J.*, **226**, 632.
Kalkofen, W., and Ulmschneider, P. 1979, *Ap. J.*, **227**, 655.
Kopp, R. A., and Holzer, T. E. 1976, *Solar Phys.*, **49**, 43.
Kulsrud, R., and Pierce, W. P. 1969, *Ap. J.*, **156**, 445.
Kuperus, M. 1965, *Rech. Astr. Obs. Utrecht*, **17**, 1.
Kwok, S. 1975, *Ap. J.*, **198**, 583.
Lerche, I., and Vasyliunas, V. M. 1976, *Ap. J.*, **210**, 85.
Linsky, J. L., and Ayres, T. R. 1978, *Ap. J.*, **220**, 619.
Linsky, J. L., and Haisch, B. M. 1979, *Ap. J. (Letters)*, **229**, L27.
Mullan, D. J. 1978, *Ap. J.*, **226**, 151.
Osterbrock, D. E. 1961, *Ap. J.*, **134**, 347.
Parker, E. N. 1958, *Ap. J.*, **128**, 644.
_____. 1963, *Interplanetary Dynamical Processes* (New York: Wiley).
_____. 1965, *Space Sci. Rev.*, **4**, 666.
Piddington, J. H. 1956, *M.N.R.A.S.*, **116**, 314.
Reid, M. J., Moran, J. M., Leach, R. W., Ball, J. A., Johnston, K. J., Spencer, J. H., and Swenson, G. W. 1979, *Ap. J. (Letters)*, **227**, L89.

Reimers, D. 1975, *Mém. Soc. Roy. Liège*, 6th Ser., **8**, 369.
_____. 1977*a*, *Astr. Ap.*, **57**, 395.
_____. 1977*b*, *Astr. Ap.*, **61**, 217.
Renzini, A., Cacciari, C., Ulmschneider, P., and Schmitz, F. 1977, *Astr. Ap.*, **61**, 39.
Rosner, R., and Vaiana, G. 1977, *Ap. J.*, **216**, 141.
Sagdeev, R. Z., and Galeev, A. A. 1969, *Nonlinear Plasma Theory* (New York: Benjamin).
Skumanich, A. 1972, *Ap. J.*, **171**, 565.
Spitzer, L. 1968, *Diffuse Matter in Space* (New York: Interscience).
Stencel, R. 1978, *Ap. J.* (*Letters*), **233**, L37.
Sutton, E. C., Storey, J. W. V., Betz, A. L., Townes, C. H., and Spears, D. L. 1977, *Ap. J.* (*Letters*), **217**, L97.
Ulmschneider, P. 1970, *Solar Phys.*, **12**, 403.
Ulmschneider, P., and Kalkofen, W. 1978, *Astr. Ap.*, **69**, 407.
Ulmschneider, P., Schmitz, F., and Hammer, L. 1979, *Astr. Ap.*, **74**, 229.
Ulmschneider, P., Schmitz, F., Renzini, A., Cacciari, C., Kalkofen, W., and Kurucz, R. 1977, *Astr. Ap.*, **61**, 515.
Vernazza, J. E., Avrett, E. A., and Loeser, R. 1973, *Ap. J.*, **184**, 605.
Wentzel, D. 1974, *Solar Phys.*, **39**, 129.
Weymann, R. 1960, *Ap. J.*, **132**, 380.
_____. 1962, *Ap. J.*, **136**, 844.
Willson, L. A., and Hill, S. J. 1979, *Ap. J.*, **228**, 854.
Wilson, O. C. 1959, *Ap. J.*, **131**, 75.
_____. 1960, *Ap. J.*, **132**, 136.
Wilson, O. C., and Abt, H. A. 1954, *Ap. J. Suppl*, **1**, 1.
Wing, R. F. 1978, in *High Resolution Spectroscopy*, *Proc.* 4*th International Colloquium on Astrophysics*, Trieste, ed. M. Hack, p. 683.
Wood, P. R. 1979, *Ap. J.*, **227**, 220.

L. HARTMANN: Center for Astrophysics, 60 Garden Street, Cambridge, MA 02138

K. B. MACGREGOR: Laboratory for Astrophysics and Space Research, University of Chicago, 933 East 56th Street, Chicago, IL 60637